

p53–Mdm2 loop controlled by a balance of its feedback strength and effective dampening using ATM and delayed feedback

J. Wagner, L. Ma, J.J. Rice, W. Hu, A.J. Levine and G.A. Stolovitzky

Abstract: When the genomic integrity of a cell is challenged, its fate is determined in part by signals conveyed by the p53 tumour suppressor protein. It was observed recently that such signals are not simple gradations of p53 concentration, but rather a counter-intuitive limit-cycle behaviour. Based on a careful mathematical interpretation of the experimental body of knowledge, we propose a model for the p53 signalling network and characterise the p53 stability and oscillatory dynamics. In our model, ATM, a protein that senses DNA damage, activates p53 by phosphorylation. In its active state, p53 has a decreased degradation rate and an enhanced transactivation of *Mdm2*, a gene whose protein product Mdm2 tags p53 for degradation. Thus the p53–Mdm2 system forms a negative feedback loop. However, the feedback in this loop is delayed, as the pool of *Mdm2* molecules being induced by p53 at a given time will mark for degradation the pool of p53 molecules at some later time, after the *Mdm2* molecules have been transcribed, exported out of the nucleus, translated and transported back into the nucleus. The analysis of our model demonstrates how this time lag combines with the ATM-controlled feedback strength and effective dampening of the negative feedback loop to produce limit-cycle oscillations. The picture that emerges is that ATM, once activated by DNA damage, makes the p53–Mdm2 oscillator undergo a supercritical Hopf bifurcation. This approach yields an improved understanding of the global dynamics and bifurcation structure of our time-delayed, negative feedback model and allows for predictions of the behaviour of the p53 system under different perturbations.

1 Introduction

The p53 tumour suppressor protein is a key regulator of a range of processes involved in the prevention of cancer formation, including cell cycle arrest, DNA repair and apoptosis [1]. Its primary *modus operandi* is to act as a transcription factor for a number of target genes, including its own negative regulator *Mdm2* [2–8], whose gene product Mdm2 acts as an E3 ubiquitin ligase for p53 [9]. In unstressed cells, Mdm2 maintains p53 at very low levels, but following cellular stress, including DNA damage caused by ionising radiation, ultraviolet light and carcinogens, this inhibition is relieved, and p53 stabilises [10–13]. In some cases, oscillations of both p53 and Mdm2 levels have been observed [14–16]. Although the biological significance of these oscillations remains unclear, they appear to involve a combination of post-translational modifications of p53 [17] and the negative feedback loop consisting of p53 transactivation of *Mdm2* and Mdm2-mediated ubiquitination of p53 [18].

DNA damage from ionising radiation involves activation of a protein kinase, ATM [19], which has been shown to bind to p53 and phosphorylate Ser₁₅ [19–21]. ATM also phosphorylates the checkpoint kinase CHK2 [22, 23], which can phosphorylate p53 at Ser₂₀ [24, 25]. Phosphorylation of both Ser₁₅ and Ser₂₀ are critical for p53 activation and stabilisation [26]. The stabilisation is achieved by a reduction of p53's interaction with Mdm2 [26–29]. Once activated, p53 binds as a tetramer [30] to the P2 promoter in intron 1 of the *Mdm2* gene [8, 31, 32], yielding a transcript that is translated approximately eight times more efficiently than that deriving from the constitutively active, p53 insensitive P1 promoter [33]. Once translated, Mdm2 binds p53 and marks it for degradation using the proteasome [34, 35], thus closing the negative feedback loop.

Several models have examined the p53 negative feedback loop in the context of oscillations observed in cell populations exposed to irradiation [14, 36, 37]. The Lev Bar-Or model explained p53 and Mdm2 oscillations in terms of a signal-dependent intermediary with slow kinetics encompassing the DNA binding and transcriptional activity of p53, including the inhibition of p53 transcriptional activity by Mdm2 binding [14]. Further hypothesising a signal-dependent p53 degradation mechanism, they found that a decaying DNA damage signal with sufficiently long timescale could generate damped oscillations. More recently, Monk used elegant models incorporating explicit time delays, representing transcription, splicing, transport and translation, to study damped and stable oscillations in three oscillatory gene expression systems: Hes1, p53 and NF- κ B [36]. Restricting his models to simple regulatory

© IEE, 2005

IEE Proceedings online no. 20050025

doi:10.1049/ip-syb:20050025

Paper first received 17th May and in final revised form 27th July 2005

J. Wagner, L. Ma, J.J. Rice and G.A. Stolovitzky are with the IBM Computational Biology Center, IBM T.J. Watson Research Center, PO Box 218, Yorktown Heights, NY 10598, USA

W. Hu and A.J. Levine are with the Cancer Institute of New Jersey, Robert Wood Johnson School of Medicine, New Brunswick, NJ, USA

A.J. Levine is also with the Institute for Advanced Study, Princeton, NJ, USA
E-mail: gustavo@us.ibm.com

mechanisms allowed Monk to argue strongly that time delays drive oscillations in these simple negative feedback systems without necessitating additional components [38, 39]. Although both of these models pointed to the importance of the time lag, neither addressed the role of ATM-mediated p53 activation in initiating and regulating oscillations [2], and it is not clear how ATM and the time lag work together to drive oscillations, if at all. Elucidation of the combined role played by both ATM and the time lag to modulate the oscillations of the p53–Mdm2 system is the main goal of the present study.

Moreover, recent evidence suggests that damped oscillations are a property only of populations of cells and arise from a summing of the individual contributions of single cells exhibiting ‘digital behaviour’ [15]. In this scenario, each cell responds to a given level of irradiation with a finite, but variable, number of fixed amplitude and fixed period oscillations. Such behaviour is consistent with a stable limit cycle oscillation of a biochemical circuit in which a DNA damage parameter drives the system through a bifurcation after irradiation [16, 38]. Although this general qualitative description provides a good starting framework, much work remains in constructing a quantitative and biologically plausible model that produces oscillations that can be switched on and off with the DNA damage level.

Recently Tyson and collaborators [40] proposed a model in which DNA damage and p53-mediated repair modulate stable oscillations arising from a combination of the $p53 \rightarrow Mdm2 \dashv p53$ negative feedback loop and the $p53 \rightarrow PTEN \dashv Akt \rightarrow Mdm2 \dashv p53$ positive feedback loop (see [18] for a description of feedback loops in the p53 network). The resulting network architecture supports limit-cycle dynamics, as does the time lagged negative feedback loop studied in this paper. Ciliberto *et al.* [40] proposed a number of experiments to elucidate which of those two mechanisms best explains the generation of oscillations. One such obvious experiment was to eliminate the positive feedback loop and see if the oscillations persisted. Interestingly, whereas PTEN is clearly induced by p53 in heart and liver tissues, PTEN is hardly induced by p53 in MCF-7 cells [41], where the digital response was observed [15]. Therefore the positive feedback loop mechanism through PTEN seems to be inactive in the very cells where the limit-cycle behaviour was observed. In spite of this preliminary result supporting the time lagged negative feedback hypothesis, more experimental work will be needed before we can rule out a positive feedback loop mechanism.

We set out to construct a model that is both consistent with known p53–Mdm2 interaction mechanisms and able to be driven into limit-cycle oscillations by a DNA damage-induced ATM signal. Moreover, our model is sufficiently parsimonious to be amenable to non-linear systems analysis, such as parameter variation studies and phase plane analysis. Generally speaking, biological systems are expected to have substantial variability, and so demonstrating robustness against parameter variation becomes crucial for any model that is claimed to be biologically plausible. The model presented here serves as a scaffold for constructing a more biologically comprehensive model [42], in which the limit-cycle behaviour studied in this paper is complemented with stochastic components to explain the phenomenology observed in [15]. However, a cost of added detail is the inability to show the full characterisation of dynamic responses that is possible with the sparser model presented here.

Building on Monk’s work [36], we incorporate a two-state model for p53, including an active p53 state that transactivates *Mdm2* and an inactive p53 state that is susceptible to Mdm2-mediated ubiquitination. From this, we then derive and analyse a reduced, two-variable model that mimics qualitatively our full model. Examination of this reduced model allows us to examine explicitly how ATM modulates key components of the system, thus switching the response between fixed points and stable limit cycles. Moreover, comparison of this reduced model with a linear negative feedback model with time lag, whose stability condition we solve analytically, yields a better understanding of how stability arises in time delayed negative feedback loops. Finally, we present an interpretation of this linear model in terms of the strength of the feedback loop and the effective dampening of oscillations underlying negative feedback systems and discuss ATM activation in this context.

2 Mathematical model

As depicted in Fig. 1a, we consider inactive and active p53 in the nucleus and *Mdm2* mRNA and Mdm2 protein in both the nucleus and cytosol. When activated by ATM, p53 increases *Mdm2* levels in the nucleus. *Mdm2* mRNA is then exported to the cytosol, where it is translated into Mdm2 protein. Cytosolic Mdm2 is then transported back into the nucleus, where it ubiquitinates p53. Consistent with the hypothesis that p53 activation inhibits complexation with Mdm2 [27], we assume active p53 ubiquitination is essentially zero. We also consider degradation pathways for p53, *Mdm2* mRNA and Mdm2 protein (not shown in the figure). In this paper, we focus on the dynamic behaviour of the model represented in Fig. 1b using active ATM as an adjustable parameter; we do not include DNA damage or repair processes, nor even ATM activation processes that we considered in detail in [42] in a stochastic context.

The p53 pathway, as encapsulated in our model, is shown in Fig. 1b. In formulating our model, we include only nuclear concentrations and introduce two explicit time lags. The time lag τ_1 encapsulates the processes (primarily, elongation and splicing) underlying the transcriptional production of mature, nuclear *Mdm2* mRNA. The second time lag τ_2 encompasses *Mdm2* transport to the cytosol, translation to protein and transport of Mdm2 protein into the nucleus, thus eliminating cytosolic *Mdm2* mRNA and Mdm2 protein concentrations from the model.

Our model extends Monk’s work [36] by incorporating a two-state model for p53. As a result, Monk’s explicit time delay and our active p53 state can be thought of as replacing the Lev Bar-Or model’s intermediary [14], which comprises

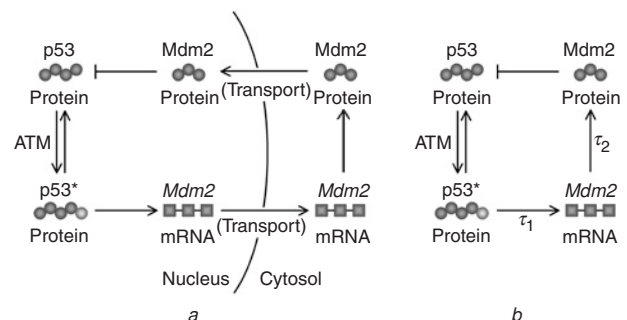


Fig. 1 Major components of the p53 pathway

a High-level schematic diagram including nuclear and cytosolic compartments

b p53 pathway as encapsulated in model (see text for details)

both an intermediate state and an implicit time delay arising from the time scale of the intermediate's kinetics. This approach puts the Lev Bar-Or intermediary on a mechanistic footing and allows us to study the effects of the intermediate state and the time lag separately. In particular, because ATM activation of p53 is fast relative to other processes [43], we can eliminate the active p53 state as a dynamic variable and leave only the time delays and slower processes as the key timescales of interest.

The full mathematical model is given in Appendix 1. In constructing this model, we have assumed a single compartment and chosen simple kinetic mechanisms wherever possible. In particular, we assume *p53* and basal *Mdm2* transcription are constant. To account for p53's preference for tetramerisation, we model the P2 promoter's dependence on p53 as a Hill function with co-operativity four [44]. The P2 promoter rate also utilises Monk's time lag τ_1 to incorporate the finite time needed for transcription; in contrast to Monk's model, however, we separate the transport and translation time lag τ_2 and include it in the equation for Mdm2 protein [45]. Finally, both ATM activation of p53 and Mdm2-mediated p53 ubiquitination are assumed to follow the usual Henri–Michaelis–Menten kinetics, consistent with an enzyme-catalysed conversion of a substrate (inactive p53) to a product (active p53 or ubiquitinated p53). All other kinetic terms are assumed to be linear, and we do not consider any potential post-transcriptional modifications [46].

In terms of the dimensionless quantities given in Appendix 1, the full model can be written as

$$\begin{aligned}\frac{dP}{dt} &= 1 - k_1 P - k_2 M \frac{P}{P + K_1} - k_p^- A \frac{P}{P + K_3} + k_p^- P^* \\ \frac{1}{k_p^-} \frac{dP^*}{dt} &= A \frac{P}{P + K_3} - P^* \\ \frac{dm}{dt} &= 1 + v_1 \frac{P^*(t - \tau_1)^4}{P^*(t - \tau_1)^4 + K_2^4} - m \\ \frac{1}{k_3} \frac{dM}{dt} &= m(t - \tau_2) - M\end{aligned}$$

where P and P^* are inactive and active p53 protein, respectively; m is mature *Mdm2* mRNA; M is Mdm2 protein; and A is activated ATM protein. Note that, for convenience, we have dropped the tilde notation denoting dimensionless quantities.

Note that k_p^- and k_3 determine the timescales of the variables P^* and M , and that dimensionless time is in terms of the *Mdm2* mRNA half-life, which we estimate to be 20–40 min [47]. The transcriptional time lag τ_1 encompasses primarily elongation and splicing. Given an elongation rate of 20 nucleotides per second [48, 49] and a splicing time of the order of a few minutes [50], we estimate τ_1 to be 25–30 min, as human Mdm2 has over 30 000 nucleotides and ten introns. The time lag τ_2 can be estimated from transport, translation and folding times. Mdm2 translation requires approximately 2 min, assuming a rate of 4 amino acids per second [51], and protein folding requires in the order of fractions of a second to minutes. Nuclear mRNA export has been estimated at 4 min [50]. Nuclear import of Mdm2 is regulated by post-translational modifications [52] and is thus harder to quantify; we assume it is roughly the same as export. This yields a transport and translation time of approximately 10 min. As a result, the dimensionless time lags are, roughly, in the order of unity.

Mdm2 and p53 protein half-lives are probably also in the order of mRNA half-lives [36, 53–55], suggesting that k_1 , k_2 and k_3 are in the order of unity. Moreover, ATM phosphorylation is probably fast relative to the timescales of mRNA and protein degradation [43]. Finally, the P2 promoter rate has been estimated to be eight times that of the P1 promoter rate [33]. All other parameters have been chosen to illustrate the features and behaviours of our model and not necessarily to match experimental data *per se* (for a set of parameters that match experimental data more closely, see [42]). With these considerations in mind, we have chosen a standard set of dimensionless parameter values, as given in Table 1; these values are used in all calculations, except where parameters are varied, or where noted otherwise. Note that, in the light of the approximations made in estimating time lags, we have chosen τ_1 and τ_2 such that the total time lag $\tau = \tau_1 + \tau_2$ is unity. It is interesting to note that the solutions for P , P^* and M depend only on the total time lag τ . Therefore, in our study below, we will consider the dependence of the solutions of our model in terms of the aggregate time lag τ .

3 Results

3.1 General results

Our model exhibits stable limit-cycle oscillations in response to increased ATM activation. As can be seen in Fig. 2a, when ATM activation is low ($A = 0.2$), the system rests at steady state. Increasing A from 0.2 to 2.0 (left arrow, at $t = 2$) induces oscillations that persist as long as ATM activation remains elevated, relaxing back to equilibrium when ATM activation is reduced to $A = 0.2$ again (right arrow, at $t = 35$). The model's response to ATM is shown more quantitatively in the bifurcation diagram in Fig. 2b: as ATM activation is increased from 0.6 to 10, oscillations arise through Hopf bifurcation at $A = 1.25$ and then disappear at a second Hopf bifurcation at $A = 3.6$.

As expected, these oscillations (both their existence and their period) are critically dependent on the total time lag τ . Figure 3a shows the bifurcation structure of the system with respect to the total time lag: for small values of τ , the system does not oscillate, but oscillations arise through Hopf bifurcation at $\tau = 0.88$. The period of oscillations also depends on the time lag, as shown in Fig. 3b. As is common in lagged systems, the period and the phase difference between p53 and Mdm2 both scale linearly as a function of τ .

Table 1: Standard set of dimensionless parameter values used in all calculations, except where parameters are varied or where noted otherwise

Parameter	Value
τ_1	0.5
τ_2	0.5
A	2
K_1	0.2
K_2	0.5
K_3	0.6
v_1	8
k_1	0.2
k_2	1
k_3	1
k_p^-	20

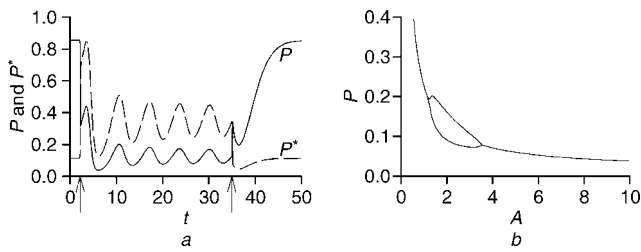


Fig. 2 Maximum and minimum values of P as A is varied over range 0.6–10

a Time series of P and P^* as A is changed from 0.2 to 2 (left arrow), and then back again from 2 to 0.2 (right arrow)
b Bifurcation diagram of full model with respect to A

3.2 Reduction of the model to two equations

Mathematical analysis can be difficult for models containing three or more variables and is further complicated by the presence of time lags. In our model, however, it should be clear that M , and possibly P^* , plays a smaller role in the model's core dynamics than do P and m . This led us to study a simpler, two-variable model, whose dynamics approximate those of the full model. Formally, assuming P^* and M are always in equilibrium with P and m ,

$$P^* = A \frac{P}{P + K_3} \quad M = m$$

the full model can be reduced to

$$\left[1 + A \frac{K_3}{(P + K_3)^2} \right] \frac{dP}{dt} = 1 - k_1 P - k_2 M \frac{P}{P + K_1}$$

$$\frac{dM}{dt} = 1 + v_1 \frac{[P(t - \tau)/(P(t - \tau) + K_3)]^4}{[P(t - \tau)/(P(t - \tau) + K_3)]^4 + (K_2/A)^4} - M$$

Note that the P equation derives from the equation for the slow variable, $P_T = P + P^*$, which under the equilibrium assumption becomes

$$P_T = P + A \frac{P}{P + K_3}$$

and that the M equation derives from the full model m equation using the equilibrium condition $M = m$. Although we could have kept the variables P_T and m , our choice allows for more direct comparison with Monk's model. As a result, all of our figures are in terms of P rather than P_T (or even P^*). However, it is useful to keep in mind that both P_T and P^* are monotonically increasing functions of both A and P .

In the reduced model, the total time lag appears in the term representing p53 transactivation of Mdm2. It should

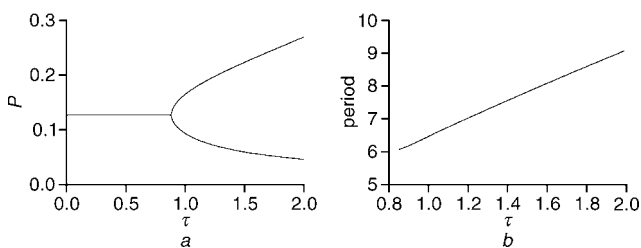


Fig. 3
a Bifurcation diagram of full model with respect to τ
 Diagram shows maximum and minimum values of P as τ is varied over range 0–2
b Period as function of τ over range of oscillatory values in Fig. 3*a*

be clear that Mdm2's 'local in time' dependence on p53 is replaced by a 'lagged in time' dependence on p53, with the lag equal to the sum of the time lags between Mdm2 and p53. As a result, despite the difference between the placement of the time lags in the full model and the time lag in Monk's model, the time lag enters the reduced model in a manner analogous to Monk's model. Indeed, reducing Monk's model to the same two variables, p53 and Mdm2 protein, yields a model similar to our reduced model (see Section 4). As a result, Monk's model and our full model differ by a slight phase shift (of magnitude τ_2) in $Mdm2$ mRNA.

3.3 Full and reduced models are qualitatively similar

Despite eliminating two of the four coupled equations, the reduced model mimics qualitatively the full model. Indeed, we have verified this with calculations, as shown in Fig. 4 by the time series (Fig. 4*a*) and phase plane plots (Fig. 4*b*): both the full (solid curves) and reduced (dashed curves) models exhibit similar limit-cycle oscillations for the standard parameter values given in Table 1.

We have also compared the global bifurcation structures by examining one-dimensional bifurcation diagrams for each parameter common to both models. As shown in Fig. 5, both the full (solid curves) and reduced (dashed curves) models behave similarly with respect to changes in each parameter. For example, both models contain a single bifurcation with respect to both τ and v_1 , and two bifurcations with respect to both A and k_2 . In all cases, the critical bifurcation values differ slightly, and the regions supporting oscillations in the full model are always larger than, and contain, those of the reduced model. This is not surprising, however, as the reduced model assumes rapid equilibration of P^* and M , and solutions have less freedom to wander from the three nullclines associated with those variables.

Agreement between the full and reduced models depends critically on the equilibrium assumptions. As ATM phosphorylation of p53 is assumed to be fast relative to dimensionless time (the time scale being $1/k_p = 0.05$), we expect P^* also to be in constant equilibrium with P . Mdm2, however, is not a fast variable, as reflected by our standard parameters ($k_3 = 1$). Despite this, the reduced model agrees sufficiently well with the full model to provide a much simpler system for analysis. As a result, our analysis of the reduced model applies to the full model as well.

3.4 Further reduction reveals additional qualitative behaviour

The other stumbling block to analysis, the time lag, can be approximated by replacing $P(t - \tau)$ with its expansion

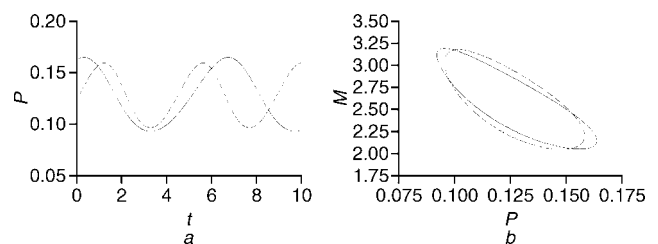


Fig. 4 Oscillatory solutions of full and reduced models
 — Full model — — Reduced model
a Time series showing P as a function of time
b Phase plane portrait of the solution in *a*
 At time $t = 0$, transients have already subsided

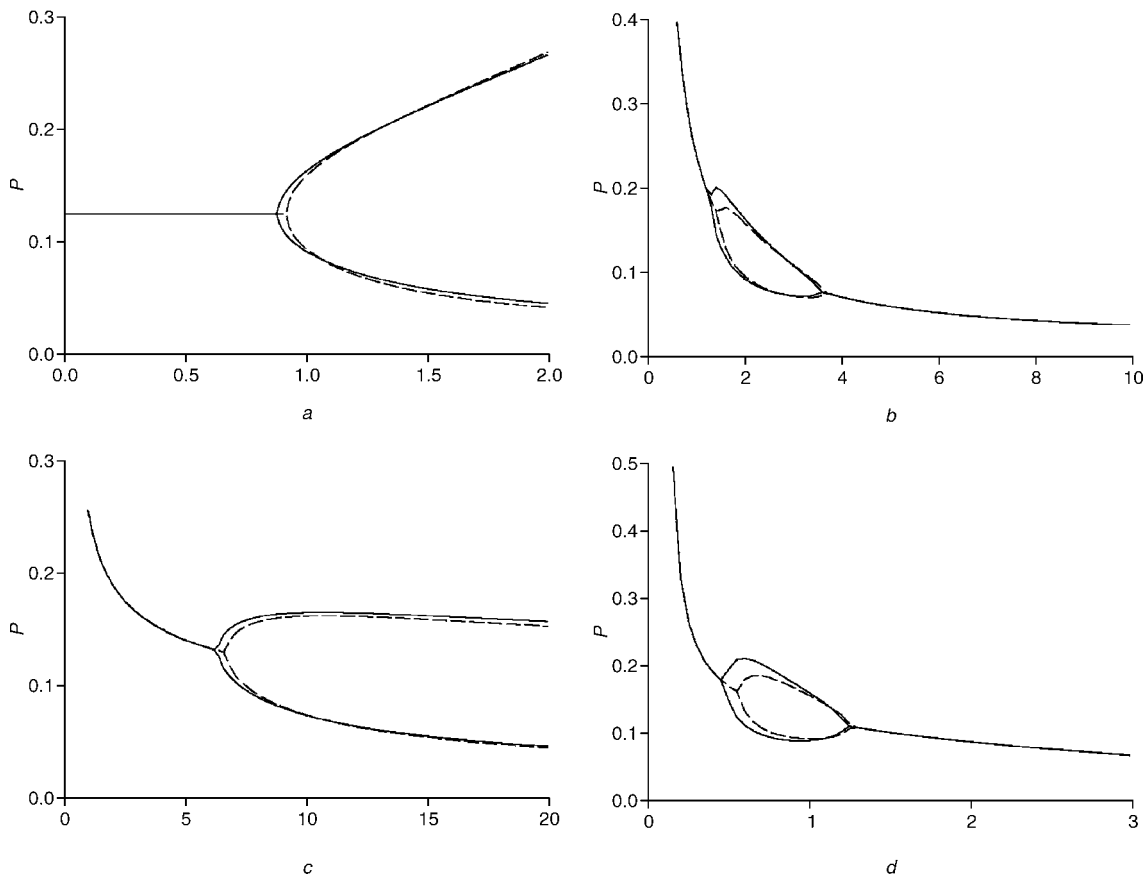


Fig. 5 Bifurcation diagrams of full and reduced models with respect to τ , A , v_1 and k_2

a τ *b* A *c* v_1 *d* k_2

Diagrams show maximum and minimum values of P as each parameter is varied over range

in terms of τ

$$\begin{aligned}
 P(t - \tau) &= P(t) - \tau P'(t) + O(\tau^2) \\
 &\approx P(t) - \tau \left[1 + A \frac{K_3}{(P(t) + K_3)^2} \right]^{-1} \\
 &\quad \times \left(1 - k_1 P(t) - k_2 M \frac{P(t)}{P(t) + K_1} \right)
 \end{aligned}$$

The resulting model is a reasonable, although not mathematically rigorous, prototype of the reduced model that lends itself more easily to analysis. Specifically, we expect the time lag to be in the order of unity, that is, too large for the expansion to hold quantitatively.

Bearing in mind that there are obvious quantitative differences, we have examined the behaviour of this prototype as a means for understanding the behaviour of the reduced and full models. Fig. 6 shows the P (dashed curve) and M (solid curves) nullclines, for $\tau = 0$ and $\tau = 1$. Also shown are the limit cycles (darker circles) for both the full and prototype models. Note that the prototype's limit cycle (outer circle) intersects the $\tau = 1$ M nullcline horizontally, as expected, but that the full model's (inner circle) does not; the discrepancy is a measure of the accuracy of the expansion in τ , and of the quantitative agreement between the models. Also note that, because fixed points are invariant with respect to time lags, both M nullclines intersect the P nullcline at the same location. This invariance ensures that both models yield the same fixed points.

It is also clear from Fig. 6 that the time lag 'rotates' the space near the fixed point. In our model, because only the M equation contains a time lag, only the M nullcline is

affected. However, it is important to note that, near the fixed point, where linear behaviour is expected, all eigenvalues and eigenvectors are modified by the time lag, even though the time lag appears only in the M equation; indeed, these modifications allow τ to modulate the stability of the fixed point. These modifications can also be seen qualitatively by examining the vector fields of the prototype when $\tau = 0$ and $\tau = 1$ (data not shown).

3.5 Simple linear model illuminates model dynamics

Although phase plane analysis of the prototype yields a qualitative understanding of the effects of the time lag, it

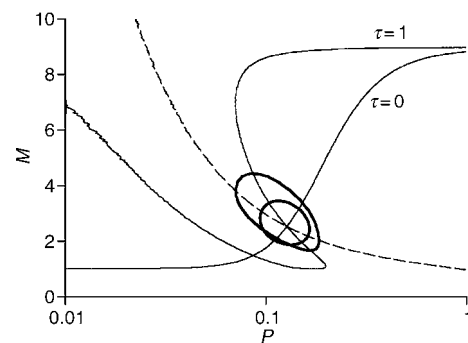


Fig. 6 Phase plane diagram of prototype model P and M nullclines, for $\tau = 0$ and $\tau = 1$ (as labelled)

Darker circles are stable limit cycles of full (inner circle) and prototype (outer circle) models
 - - - P ——— M

is insufficient to characterise quantitatively how the time lag generates stable limit cycles. To address this question, we have examined the stability near the fixed point of the reduced model.

The stability of our reduced model near the fixed point is governed by a linear system with a single time lag, with instability at the fixed point giving rise to stable limit cycle oscillations. We have examined therefore the stability of a two-variable linear system with a time lag

$$\begin{aligned} u' &= -\lambda_1 u - \omega_1 v \\ v' &= \omega_2 u(t - \tau) - \lambda_2 v \end{aligned}$$

as a means for better understanding the effects of the time lag and the global bifurcation structure of our model. In Appendix 2, we outline the derivation of the condition of marginal stability for this linear ‘ λ - ω model’

$$\tau\omega = f(\lambda_1/\omega, \lambda_2/\omega)$$

where

$$f(\lambda_1/\omega, \lambda_2/\omega)$$

$$= 2 \frac{\arcsin \sqrt{\frac{[(\lambda_1 + \lambda_2)/2\omega]^2 - 1/2}{\sqrt{1 + 4[(\lambda_1 + \lambda_2)/2\omega]^2}[(\lambda_1 - \lambda_2)/2\omega]^2 - 1}}}{\sqrt{\frac{1 + 4[(\lambda_1 + \lambda_2)/2\omega]^2[(\lambda_1 - \lambda_2)/2\omega]^2}{-[(\lambda_1 + \lambda_2)/2\omega]^2 - [(\lambda_1 - \lambda_2)/2\omega]^2}}}$$

and $\omega^2 = \omega_1\omega_2$. For each value of λ_1/ω and λ_2/ω , this condition defines a critical value of $\tau\omega$, so that, when $\tau\omega > f(\lambda_1/\omega, \lambda_2/\omega)$, solutions of the λ - ω model are unstable, corresponding to stable limit-cycle oscillations in the reduced model. Three contours ($\tau\omega = 0.1, 1$ and 10) of this surface are shown in Fig. 7. Note that the λ - ω model is always stable when $\tau = 0$, supporting our observation that the reduced model does not oscillate stably in the absence of a time lag. When the lag is non-zero, however, the λ - ω model becomes unstable for a range of values of λ_1/ω and λ_2/ω , and this range increases with increasing $\tau\omega$.

Also shown in Fig. 7 is the boundary (solid, unlabelled curve) of the region $\lambda_1\lambda_2 < \omega^2$, where the condition of marginal stability is defined; outside this region, the marginal stability condition has no solution, as $f(\lambda_1/\omega, \lambda_2/\omega) \rightarrow \infty$

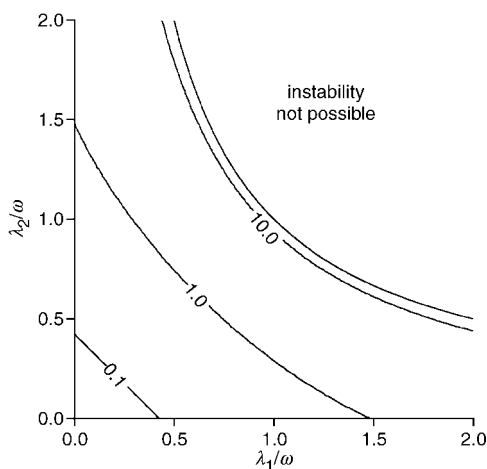


Fig. 7 Contour plot of stability condition for λ - ω model

Three contours (0.1, 1 and 10) are shown, of $\tau\omega$ as function of λ_1/ω and λ_2/ω . Unlabelled solid curve is boundary of region where stability condition is defined

as $\lambda_1\lambda_2 \rightarrow \omega^2$, and only damped oscillations are possible. This additional restriction motivates an interpretation of the stability as a balance between the feedback strength ($\omega_1\omega_2$) and the effective dampening of oscillations (λ_1 and λ_2) underlying negative feedback. If we consider stable limit cycle oscillations as the nominal, or observed, biological response, then we can interpret ω_1 and ω_2 as controlling the extent to which one mode (say v) activates the other mode (u). (Notice that u activates v , i.e. u forces v away from its fixed point, during the phases of the oscillations when $uv > 0$, but these roles are interchanged when $uv < 0$.) In like manner, λ_1 and λ_2 effectively dampen the oscillatory response. This suggests that the quantity $\lambda_1\lambda_2/\omega^2$ represents the level of dampening to activation of the oscillatory behaviour. In this interpretation, the strength of the feedback loop (activation of one mode by the other) must exceed dampening for the reduced model to exhibit stable limit cycle oscillations. Moreover, as can also be seen in Fig. 7, increasing the strength of feedback or decreasing effective dampening reduces the time lag necessary for oscillations. However, because ω also scales time in the λ - ω model, increasing feedback strength has the additional effect of increasing the dimensionless time lag $\tau\omega$, consistent with the notion that increasing the time lag decreases stability.

In our model, the fixed point is independent of τ , and so changing τ does not modify λ_1, λ_2 or ω . As a result, we would expect the bifurcation with respect to τ observed in Fig. 3a: as τ is increased from very low to very high, the system undergoes a single Hopf bifurcation as $\tau\omega$ moves above the critical value. Varying other parameters, however, generates more complicated changes in terms of λ_1, λ_2 and ω and therefore requires more detailed analysis. For example, although it may be intuitive to think of increasing ATM as always increasing activation in the p53 negative feedback loop, Fig. 2b suggests a more subtle and complicated picture.

The λ - ω model provides a model for understanding the conditions of ATM-mediated oscillations in the reduced model. To simplify the discussion, we first note that, when the reduced model is linearised, we find that $\partial M'/\partial M = -1$, so that λ_2 is 1. If we then fix $\tau = 1$ as in the standard parameters, the stability condition becomes a function of ω and $\lambda = \lambda_1$ only, specifically, the curve defined by $\omega = f(\lambda/\omega, 1/\omega)$. If we now consider the reduced model's fixed point as being a function of ATM, say $(P_0(A), M_0(A))$, then linearising around the fixed point and varying ATM parameterises a curve, $(\omega(P_0(A), M_0(A)), \lambda(P_0(A), M_0(A)))$ in the ω - λ plane.

With this in mind, we have plotted both the marginal stability curve (solid curve) and the parameterised curve (dashed curve) in Fig. 8a, for ATM varying between 0.4 and 10. In terms of our feedback strength/effective dampening interpretation, we see that increasing ATM increases the feedback strength to an effective dampening level when ATM is low, and increases the effective dampening to feedback strength level when ATM is high. The six points (a-f) correspond to the points in the ATM bifurcation diagram in Fig. 8B: low and high ATM values of (a) 0.4 and (f) 10; full model (b) low and (e) high bifurcation points; and reduced model (c) low and (d) high bifurcation points. As is clear from this figure, as ATM is increased from (a) 0.4 to (f) 10, both the full and reduced models enter and then exit the region of instability (to the right of the stability curve). Note, however, that the reduced model's bifurcation points (c and d) intersect the stability curve exactly, whereas the full model's bifurcation points lie slightly to the left of the stability curve. This

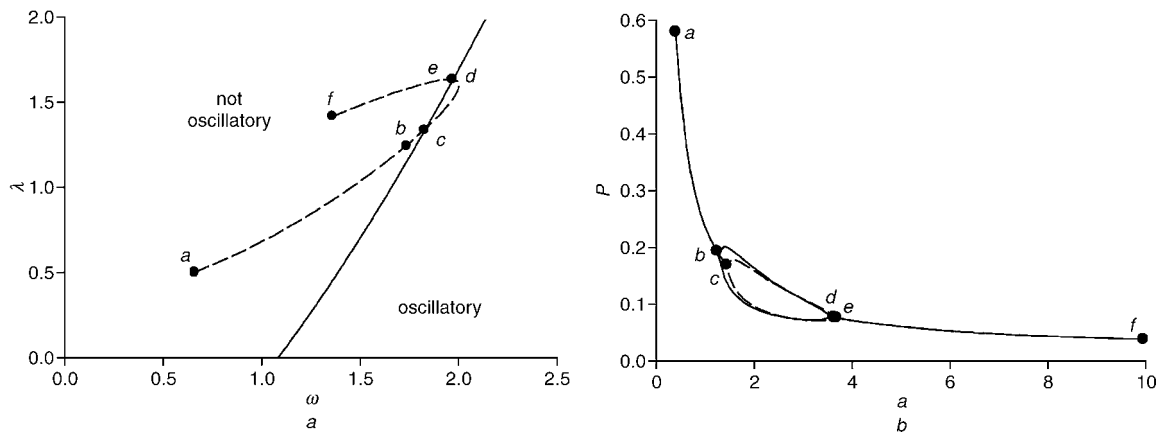


Fig. 8

a Plot of stability and parameterised curves for ATM varying between 0.4 and 10

— Stability curve - - - Parameterised curve

Six points (*a*–*f*) correspond to points in ATM bifurcation diagram in Fig. 8*b*: low and high ATM values of *a* 0.4 and *f* 10; full model *b* low and *e* high bifurcation points; and reduced model *c* low and *d* high bifurcation points. Points *d* and *e* are almost indistinguishable

b Bifurcation diagram of full and reduced models with respect to *a*

— Full model - - - Reduced model

Diagram shows maximum and minimum values of *P* as *A* is varied over range 0.4–10. Labelled points are as in Fig. 8*a*. Points *d* and *e* are almost indistinguishable

discrepancy is a result of the rapid equilibrium assumptions made in the derivation of the reduced model, which do not hold exactly in the full model. Indeed, we have verified this by increasing k_3 in the full model (data not shown).

Because ω also scales time in the λ – ω model, changing ATM also has the effect of modulating the dimensionless time lag $\tau\omega$. As a result, whenever ATM changes yield increases in feedback strength, there is a simultaneous increase in the effective time lag. Our model thus demonstrates that ATM controls the p53–Mdm2 response by modulating the time lag and the balance between the feedback strength and dampening.

4 Discussion

We have presented a time-delayed model for the p53–Mdm2 negative feedback oscillator that exhibits stable, limit-cycle oscillations in response to DNA damage. In our model, ATM phosphorylates and activates p53, leading to increased transactivation of *Mdm2* and decreased p53 ubiquitination. The analysis of our model suggests how a time lag combines with the feedback strength and dampening processes of a negative feedback loop to produce stable oscillations. This approach provides a framework to understand the global dynamics and bifurcation structure of our time-delayed, negative feedback model.

In our model, increasing ATM induces oscillations by both increasing the feedback strength and decreasing dampening of the stable limit-cycle oscillations characterising the single cell response. In the absence of ATM activation (by DNA damage signals), active p53 levels are not sufficient to activate *Mdm2* transcription, and dampening dominates. When ATM is activated sufficiently, however, *Mdm2* transcription is increased, p53 ubiquitination is decreased, and oscillations result from a shift towards enhanced feedback strength. However, there is a limit: when ATM is increased too much, oscillations cease, and only a stable fixed point is possible. In this case, ATM has effectively eliminated the Mdm2 mediated degradation of p53 by shifting too much p53 to the active state, and dampening again dominates. Thus, at this high ATM fixed point, active p53, total p53 and Mdm2 levels are high, but inactive p53 levels are low. In terms of the negative feedback loop, at low ATM, p53 activation of Mdm2 is

‘cut’, whereas, at high ATM, Mdm2 inhibition of p53 is ‘cut’. Both cases correspond to an effective reduction in the feedback strength.

Here we have argued that the nominal response to DNA damage-induced activation of ATM is to increase feedback strength and reduce dampening, thereby shifting the cellular state above a low ATM bifurcation point (see Fig. 2*b*). In some cells, however, this bifurcation point may not exist, for example, in ATM deficient or mutated cells, and thus a normal response is prevented. In nominal cells, on the other hand, it may not be possible to observe the high ATM bifurcation point, even at ATM saturating levels of DNA damage. At very high levels of DNA damage, we expect ATM activation to saturate; in this case, active ATM would be determined by the total ATM concentration. Indeed, it is possible, if not likely, that total ATM is controlled in such a way that cells always respond with oscillations, even when ATM activation is saturated. In this case, the high ATM bifurcation point would not normally be observed. The model predicts, however, that this point exists, and it may be possible to destroy oscillations at high levels of DNA damage, for example, by over-expression of ATM, or, because the dimensionless parameter *A* represents the level of activated ATM relative to the equilibrium constant of the ATM–p53 reaction (see the scaling relationships in Appendix 1), by decreasing the ATM–p53 equilibrium constant.

Our model includes ATM as a parameter, rather than a dynamic variable. Although this allows for simpler analysis of the effects of ATM activation on the underlying negative feedback system, we have also examined an extended model incorporating ATM activation and inactivation as dynamic variables. We have also explored other mechanisms for both ATM activation of p53 and Mdm2 ubiquitination of p53, including linear functions and Hill functions with higher co-operativity. In all of the model variations we have examined, ATM activation was able to initiate stable limit cycle oscillations by activating p53 and relieving Mdm2 inhibition of p53. We also stress that our analysis extends easily to these model variations; in models incorporating ATM dynamics, ATM activation and inactivation were also treated as fast processes, again resulting in a two-variable model for *P* and *M* that could be analysed using our approach.

Our model extends Monk's model [36] by including an ATM-dependent, two-state p53 model. Indeed, treating Monk's Mdm2 protein as a fast variable yields a dimensionless two-variable model that can be written, using our notation, as

$$\frac{dP}{dt} = 1 - k_1 P - k_2 P \frac{M^2}{M^2 + K_1^2}$$

$$\frac{dM}{dt} = 1 + v_1 \frac{P(t - \tau)^n}{P(t - \tau)^n + K_2^n} - M$$

Ignoring the difference in the p53 ubiquitination term for the moment, Monk's model is identical to our reduced model when P^* is taken to be a constant fraction of P . The way in which ATM enters our model, as seen in the reduced model, is to modify non-linearly the fraction of inactive p53. This scales the p53 equation, while maintaining the p53 nullcline, and modifies the Mdm2 equation by replacing p53 with active p53, scaling non-linearly the binding constant of transactivation. Therefore our study can be used to better understand the results of Monk's model, which, when interpreted in this manner, includes the two states of p53. In reference to the p53 ubiquitination term, we chose to treat p53 ubiquitination by Mdm2 as an enzymatic reaction, with p53 the substrate and Mdm2 the ligase. Instead, Monk chose a Hill function with Hill coefficient 2. In the range of parameters explored, the two representations of the same reaction give the same qualitative results.

There is experimental evidence that suggests that p53 exists primarily as a tetramer, or equivalently as a dimer of a dimer [56], and that Ser₁₅ and Ser₂₀ phosphorylation requires tetramerisation [26]. Even though the field is still controversial in this respect, it is clear that tetramerisation is necessary for p53 transactivation of its targets. In our model, p53 exists primarily as a monomer, and it is the p53 monomer that is either active or inactive. This allows us to treat tetramerisation through co-operativity in the *Mdm2* transcription term, rather than including additional intermediate p53 states. Although a more detailed model of p53 tetramerisation and activation is of interest, the current model addresses p53 activation and tetramerisation in a manner that is more amenable to analysis, allowing for simpler examination of the effects of ATM and p53 activation on the underlying dynamics. This aspect of our model might need to change as more information about the tetrameric states of DNA-unbound p53 becomes available.

Finally, we note that we have examined a large number of variations of our model to ensure model robustness. For example, we have explored other kinetics for ATM activation of p53 and Mdm2 ubiquitination of p53 and considered the effects of adding both Mdm2-dependent and Mdm2-independent ubiquitination of active p53. We have also explored different dimer and tetramer states for p53. In all cases, our model was robust to such changes, and our conclusions did not change: ATM activation can generate stable limit-cycle oscillations both by increasing the effective time lag and by controlling the balance between feedback strength and effective dampening.

5 Acknowledgments

We thank Yuhai Tu, Gyan Bhanot, Zhaohui Feng and Nicholas Hernjak for many useful discussions. We also acknowledge valuable input from our anonymous referees.

J. Wagner dedicates this manuscript to the memory of Carris 'Rad' Radcliff.

6 References

- Lane, D.P.: 'Cancer. p53, guardian of the genome', *Nature*, 1992, **358**, (6381), pp. 15–16
- Levine, A.J.: 'p53, the cellular gatekeeper for growth and division', *Cell*, 1997, **88**, (3), pp. 323–331
- Vogelstein, B., Lane, D., and Levine, A.J.: 'Surfing the p53 network', *Nature*, 2000, **408**, (6810), pp. 307–310
- Ryan, K.M., Phillips, A.C., and Vousden, K.H.: 'Regulation and function of the p53 tumor suppressor protein', *Curr. Opin. Cell Biol.*, 2001, **13**, (3), pp. 332–337
- Mayo, L.D., and Donner, D.B.: 'The PTEN, Mdm2, p53 tumor suppressor-oncoprotein network', *Trends Biochem. Sci.*, 2002, **27**, (9), pp. 462–467
- Haupt, S., Louriya-Hayon, I., and Haupt, Y.: 'p53 licensed to kill? Operating the assassin', *J. Cell Biochem.*, 2003, **88**, (1), pp. 76–82
- Michael, D., and Oren, M.: 'The p53-Mdm2 module and the ubiquitin system', *Semin. Cancer Biol.*, 2003, **13**, (1), pp. 49–58
- Wu, X., Bayle, J.H., Olson, D., and Levine, A.J.: 'The p53-Mdm2 autoregulatory feedback loop', *Genes Dev.*, 1993, **7**, (7A), pp. 1126–1132
- Honda, R., Tanaka, H., and Yasuda, H.: 'Oncoprotein Mdm2 is a ubiquitin ligase E3 for tumor suppressor p53', *FEBS Lett.*, 1997, **420**, (1), pp. 25–27
- Ashcroft, M., and Vousden, K.H.: 'Regulation of p53 stability', *Oncogene*, 1999, **18**, (5), pp. 7637–7643
- Haupt, Y., Maya, R., Kazaz, A., and Oren, M.: 'Mdm2 promotes the rapid degradation of p53', *Nature*, 1997, **387**, (6630), pp. 296–299
- Kubbutat, M.H., Jones, S.N., and Vousden, K.H.: 'Regulation of p53 stability by Mdm2', *Nature*, 1997, **387**, (6630), pp. 299–303
- Lohrum, M.A., and Vousden, K.H.: 'Regulation and activation of p53 and its family members', *Cell Death Differ.*, 1999, **6**, (12), pp. 1162–1168
- Lev Bar-Or, R., Maya, R., Segel, L.A., Alon, U., Levine, A.J., and Oren, M.: 'Generation of oscillations by the p53-Mdm2 feedback loop: a theoretical and experimental study', *Proc. Natl. Acad. Sci. USA*, 2000, **97**, (21), pp. 11250–11255
- Lahav, G., Rosenfeld, N., Sigal, A., Geva-Zatorsky, N., Levine, A.J., Elowitz, M.B., *et al.*: 'Dynamics of the p53-Mdm2 feedback loop in individual cells', *Nat. Genet.*, 2004, **36**, (2), pp. 147–150
- Tyson, J.J.: 'Monitoring p53's pulse', *Nat. Genet.*, 2004, **36**, (2), pp. 113–114
- Appella, E., and Anderson, C.W.: 'Post-translational modifications and activation of p53 by genotoxic stresses', *Eur. J. Biochem.*, 2001, **268**, (10), pp. 2764–2772
- Harris, S.L., and Levine, A.J.: 'The p53 pathway: positive and negative feedback loops', *Oncogene*, 2005, **24**, (17), pp. 2899–2908
- Canman, C.E., Lim, D.S., Cimprich, K.A., Taya, Y., Tamai, K., Sakaguchi, K., *et al.*: 'Activation of the ATM kinase by ionizing radiation and phosphorylation of p53', *Science*, 1998, **281**, (5383), pp. 1677–1679
- Banin, S., Moyal, L., Shieh, S., Taya, Y., Anderson, C.W., Chessa, L., *et al.*: 'Enhanced phosphorylation of p53 by ATM in response to DNA damage', *Science*, 1998, **281**, (5383), pp. 1674–1677
- Sarkaria, J.N., Busby, E.C., Tibbetts, R.S., Roos, P., Taya, Y., Karnitz, L.M., *et al.*: 'Inhibition of ATM and ATR kinase activities by the radiosensitizing agent, caffeine', *Cancer Res.*, 1999, **59**, (17), pp. 4375–4382
- Ahn, J.Y., Schwarz, J.K., Piwnicka-Worms, H., and Canman, C.E.: 'Threonine 68 phosphorylation by ataxia telangiectasia mutated is required for efficient activation of Chk2 in response to ionizing radiation', *Cancer Res.*, 2000, **60**, (21), pp. 5934–5936
- Matsuoka, S., Rotman, G., Ogawa, A., Shiloh, Y., Tamai, K., and Elledge, S.J.: 'Ataxia telangiectasia-mutated phosphorylates Chk2 in vivo and in vitro', *Proc. Natl. Acad. Sci. USA*, 2000, **97**, (19), pp. 10389–10394
- Chehab, N.H., Malikzay, A., Appel, M., and Halazonetis, T.D.: 'Chk2/hCds1 functions as a DNA damage checkpoint in G(1) by stabilizing p53', *Genes Dev.*, 2000, **14**, (3), pp. 278–288
- Hirao, A., Kong, Y.Y., Matsuoka, S., Wakeham, A., Ruland, J., Yoshida, H., *et al.*: 'DNA damage-induced activation of p53 by the checkpoint kinase Chk2', *Science*, 2000, **287**, (5459), pp. 1824–1827
- Shieh, S.Y., Taya, Y., and Prives, C.: 'DNA damage-inducible phosphorylation of p53 at N-terminal sites including a novel site, Ser20, requires tetramerization', *Embo. J.*, 1999, **18**, (7), pp. 1815–1823
- Shieh, S.Y., Ikeda, M., Taya, Y., and Prives, C.: 'DNA damage-induced phosphorylation of p53 alleviates inhibition by MDM2', *Cell*, 1997, **91**, (3), pp. 325–334

28 Chehab, N.H., Malikzay, A., Stavridi, E.S., and Halazonetis, T.D.: ‘Phosphorylation of Ser-20 mediates stabilization of human p53 in response to DNA damage’, *Proc. Natl. Acad. Sci. USA*, 1999, **96**, (24), pp. 13777–13782

29 Unger, T., Juven-Gershon, T., Moallem, E., Berger, M., Vogt Sionov, R., Lozano, G., *et al.*: ‘Critical role for Ser20 of human p53 in the negative regulation of p53 by Mdm2’, *Embo. J.*, 1999, **18**, (7), pp. 1805–1814

30 Waterman, J.L., Shenk, J.L., and Halazonetis, T.D.: ‘The dihedral symmetry of the p53 tetramerization domain mandates a conformational switch upon DNA binding’, *Embo. J.*, 1995, **14**, (3), pp. 512–519

31 Juven, T., Barak, Y., Zauberman, A., George, D.L., and Oren, M.: ‘Wild type p53 can mediate sequence-specific transactivation of an internal promoter within the mdm2 gene’, *Oncogene*, 1993, **8**, (12), pp. 3411–3416

32 Zauberman, A., Flusberg, D., Haupt, Y., Barak, Y., and Oren, M.: ‘A functional p53-responsive intronic promoter is contained within the human mdm2 gene’, *Nucleic Acids Res.*, 1995, **23**, (14), pp. 2584–2592

33 Landers, J.E., Cassel, S.L., and George, D.L.: ‘Translational enhancement of mdm2 oncogene expression in human tumor cells containing a stabilized wild-type p53 protein’, *Cancer Res.*, 1997, **57**, (16), pp. 3562–3568

34 Fuchs, S.Y., Adler, V., Buschmann, T., Wu, X., and Ronai, Z.: ‘Mdm2 association with p53 targets its ubiquitination’, *Oncogene*, 1998, **17**, (19), pp. 2543–2547

35 Fang, S., Jensen, J.P., Ludwig, R.L., Vousden, K.H., and Weissman, A.M.: ‘Mdm2 is a RING finger-dependent ubiquitin protein ligase for itself and p53’, *J. Biol. Chem.*, 2000, **275**, (12), pp. 8945–8951

36 Monk, N.A.: ‘Oscillatory expression of Hes1, p53, and NF-kappaB driven by transcriptional time delays’, *Curr. Biol.*, 2003, **13**, (16), pp. 1409–1413

37 Tiana, G., Jensen, M.H., and Sneppen, K.: ‘Time delay as a key to apoptosis induction in the p53 network’, *Eur. Phys. J. B.*, 2002, **29**, pp. 135–140

38 Griffith, J.S.: ‘Mathematics of cellular control processes. I. Negative feedback to one gene’, *J. Theor. Biol.*, 1968, **20**, (2), pp. 202–208

39 Tyson, J.J., Chen, K.C., and Novak, B.: ‘Sniffers, buzzers, toggles and blinkers: dynamics of regulatory and signaling pathways in the cell’, *Curr. Opin. Cell. Biol.*, 2003, **15**, (2), pp. 221–231

40 Ciliberto, A., Novak, B., and Tyson, J.: ‘Steady states and oscillations in the p53/Mdm2 network’, *Cell Cycle*, 2005, **4**, (3), pp. 488–493

41 Feng, Z., Levine, A.J.: Unpublished. Personal communication, 2005.

42 Ma, L., Wagner, J., Rice, J.J., Hu, W., Levine, A.J., and Stolovitzky, G.: ‘A plausible model for the digital response of p53 to DNA damage’, *Proc. Natl. Acad. Sci., USA*, 2005, **102**, (40), pp. 14266–14271

43 Bakkenist, C.J., and Kastan, M.B.: ‘DNA damage activates ATM through intermolecular autophosphorylation and dimer dissociation’, *Nature*, 2003, **421**, (6922), pp. 499–506

44 Weinberg, R.L., Veprintsev, D.B., and Fersht, A.R.: ‘Cooperative binding of tetrameric p53 to DNA’, *J. Mol. Biol.*, 2004, **341**, (5), pp. 1145–1159

45 Mahaffy, J.M., and Pao, C.V.: ‘Models of genetic control by repression with time delays and spatial effects’, *J. Math. Biol.*, 1984, **20**, (1), pp. 39–57

46 Hsing, A., Faller, D.V., and Vaziri, C.: ‘DNA-damaging aryl hydrocarbons induce Mdm2 expression via p53-independent post-transcriptional mechanisms’, *J. Biol. Chem.*, 2000, **275**, (34), pp. 26024–26031

47 Wang, Y., Liu, C.L., Storey, J.D., Tibshirani, R.J., Herschlag, D., and Brown, P.O.: ‘Precision and functional specificity in mRNA decay’, *Proc. Natl. Acad. Sci. USA*, 2002, **99**, (9), pp. 5860–5865

48 Ucker, D.S., and Yamamoto, K.R.: ‘Early events in the stimulation of mammary tumor virus RNA synthesis by glucocorticoids. Novel assays of transcription rates’, *J. Biol. Chem.*, 1984, **259**, (12), pp. 7416–7420

49 O’Brien, T., and Lis, J.T.: ‘Rapid changes in Drosophila transcription after an instantaneous heat shock’, *Mol. Cell. Biol.*, 1993, **13**, (6), pp. 3456–3463

50 Audibert, A., Weil, D., and Dautry, F.: ‘In vivo kinetics of mRNA splicing and transport in mammalian cells’, *Mol. Cell. Biol.*, 2002, **22**, (19), pp. 6706–6718

51 Lodish, H., Berk, A., Zipursky, S.L., Matsudaira, P., Baltimore, D., and Darnell, J.E.: ‘Molecular Cell Biology’ (W. H. Freeman and Co., New York, 2000, 4th edn.)

52 Meek, D.W., and Knippschild, U.: ‘Posttranslational modification of MDM2’, *Mol. Cancer Res.*, 2003, **1**, (14), pp. 1017–1026

53 Giaccia, A.J., and Kastan, M.B.: ‘The complexity of p53 modulation: emerging patterns from divergent signals’, *Genes Dev.*, 1998, **12**, (19), pp. 2973–2983

54 Okumura, N., Saji, S., Eguchi, H., Hayashi, S., Saji, S., and Nakashima, S.: ‘Estradiol stabilizes p53 protein in breast cancer cell line, MCF-7’, *Jpn. J. Cancer Res.*, 2002, **93**, (8), pp. 867–873

55 Hui, L., Abbas, T., Pielak, R.M., Joseph, T., Bargonetti, J., and Foster, D.A.: ‘Phospholipase D elevates the level of MDM2 and suppresses DNA damage-induced increases in p53’, *Mol. Cell. Biol.*, 2004, **24**, (13), pp. 5677–5686

56 Clore, G.M., Omichinski, J.G., Sakaguchi, K., Zambrano, N., Sakamoto, H., Appella, E., *et al.*: ‘High-resolution structure of the oligomerization domain of p53 by multidimensional NMR’, *Science*, 1994, **265**, (5170), pp. 386–391

7 Appendices

7.1 Mathematical model

From Fig. 1 and the discussion in the text, our model can be written

$$\frac{dP}{dt} = v_3 - k_1 P - k_2 M \frac{P}{P + K_1} - k_p^+ A \frac{P}{P + K_3} + k_p^- P^*$$

$$\frac{dP^*}{dt} = k_p^+ A \frac{P}{P + K_3} - k_p^- P^*$$

$$\frac{dm}{dt} = v_1 + v_2 \frac{P^*(t - \tau_1)^4}{P^*(t - \tau_1)^4 + K_2^4} - k_3 m$$

$$\frac{dM}{dt} = k_4 m(t - \tau_2) - k_5 M$$

where P and P^* are inactive and active p53 protein, respectively; m is *Mdm2* mRNA; M is *Mdm2* protein; and A is active ATM protein.

In the analysis of our model, it is useful to work with dimensionless units. Throughout this manuscript, then, we use the dimensionless quantities defined by the scaling relationships:

$$\begin{aligned} \tilde{t} &= k_3 t & \tilde{\tau}_1 &= k_3 \tau_1 & \tilde{\tau}_2 &= k_3 \tau_2 \\ \tilde{P} &= \frac{k_3}{v_3} P & \tilde{K}_1 &= \frac{k_3}{v_3} K_1 & \tilde{k}_1 &= \frac{k_1}{k_3} \\ \tilde{P}^* &= \frac{k_3}{v_3} P^* & \tilde{K}_2 &= \frac{k_3}{v_3} K_2 & \tilde{k}_2 &= \frac{k_2 k_4 v_1}{k_3 k_5 v_3} \\ \tilde{m} &= \frac{k_3}{v_1} m & \tilde{K}_3 &= \frac{k_3}{v_3} K_3 & \tilde{k}_3 &= \frac{k_5}{k_3} \\ \tilde{M} &= \frac{k_3 k_5}{k_4 v_1} M & \tilde{v}_1 &= \frac{v_2}{v_1} & \tilde{k}_p^- &= \frac{k_p^-}{k_3} \\ \tilde{A} &= \frac{k_3 k_p^+}{v_3 k_p^-} A \end{aligned}$$

Note that \tilde{k}_3 and \tilde{k}_p^- appear only in the full model, and that $\tilde{\tau}_1$ and $\tilde{\tau}_2$ appear in the reduced model as $\tilde{\tau} = \tilde{\tau}_1 + \tilde{\tau}_2$.

7.2 λ - ω model

In this section, we examine the stability of a two-variable linear system with a single time lag

$$\begin{aligned} u' &= -\lambda_1 u - \omega_1 v(t - \tau_1) \\ v' &= \omega_2 u(t - \tau_2) - \lambda_2 v \end{aligned}$$

for positive λ_1 , λ_2 , ω_1 and ω_2 , as might be expected near the fixed point of the reduced model. Our choice of this model also derives from our interpretation that ω_1 and ω_2 represent feedback strength, and λ_1 and λ_2 represent dampening, in a negative feedback loop.

The stability at the fixed point (0, 0) can be found by seeking solutions of the form $u(t) = A \exp(st)$, $v(t) = B \exp(st)$. Substituting yields, in matrix form,

$$\begin{pmatrix} s + \lambda_1 & \omega_1 e^{-s\tau_1} \\ -\omega_2 e^{-s\tau_2} & s + \lambda_2 \end{pmatrix} \begin{pmatrix} A \\ B \end{pmatrix} = \begin{pmatrix} 0 \\ 0 \end{pmatrix}$$

This has a solution when the determinant of the matrix vanishes

$$(s + \lambda_1)(s + \lambda_2) + \omega^2 e^{-s\tau} = 0$$

where $\omega^2 = \omega_1 \omega_2$ and $\tau = \tau_1 + \tau_2$. Note that the stability condition is a function only of the added time lags. Therefore the λ - ω model presented in Section 3.5 is a special case ($\tau_1 = 0$ and $\tau_2 = \tau$) of that presented here but has the same stability features.

The boundary between decaying and non-decaying solutions occurs when $\text{Re } s = 0$, and so we seek solutions of the form $s = yi$. Substituting and equating real and

imaginary parts yield

$$\cos(\tau y) = y^2 + \left(\frac{\lambda_1 - \lambda_2}{2\omega}\right)^2 - \left(\frac{\lambda_1 + \lambda_2}{2\omega}\right)^2$$

$$\sin(\tau y) = 2\left(\frac{\lambda_1 + \lambda_2}{2\omega}\right)y$$

These two equations can be combined to eliminate y , yielding the condition for marginal stability of the lagged λ - ω model

$$\tau\omega = 2 \frac{\arcsin \sqrt{\frac{[(\lambda_1 + \lambda_2)/2\omega]^2 - 1/2}{\times [\sqrt{1 + 4[(\lambda_1 + \lambda_2)/2\omega]^2} [(\lambda_1 - \lambda_2)/2\omega]^2 - 1]}}}{\sqrt{\frac{\sqrt{1 + 4[(\lambda_1 + \lambda_2)/2\omega]^2} [(\lambda_1 - \lambda_2)/2\omega]^2}{-[(\lambda_1 + \lambda_2)/2\omega]^2 - [(\lambda_1 - \lambda_2)/2\omega]^2}}}}$$

Note that, because $\arcsin(x)$ is only defined for $-1 < x < 1$, and the denominator must be real, the condition for marginal stability of the λ - ω model is only valid when $\lambda_1 \lambda_2 < \omega^2$.